PHYSICAL REVIEW B **87**, 140406(R) (2013)

Magnetic and crystal structures of Sr_2IrO_4: A neutron diffraction study

Feng Ye,[1,2] Songxue Chi,[1] Bryan C. Chakoumakos,[1] Jaime A. Fernandez-Baca,[1,3] Tongfei Qi,[2] and G. Cao[2]
[1]*Quantum Condensed Matter Division, Oak Ridge National Laboratory, Oak Ridge, Tennessee 37831, USA*
[2]*Center for Advanced Materials, Department of Physics and Astronomy, University of Kentucky, Lexington, Kentucky 40506, USA*
[3]*Department of Physics and Astronomy, University of Tennessee, Knoxville, Tennessee 37996, USA*
(Received 11 February 2013; published 22 April 2013)

We report a single-crystal neutron diffraction study of the layered Sr_2IrO_4. This work unambiguously determines the magnetic structure of the system and reveals that the spin orientation rigidly tracks the staggered rotation of the IrO_6 octahedra in Sr_2IrO_4. The long-range antiferromagnetic order has a canted spin configuration with an ordered moment of 0.208(3) μ_B/Ir site within the basal plane; a detailed examination of the spin canting yields 0.202(3) and 0.049(2) μ_B/site for the a axis and the b axis, respectively. It is intriguing that forbidden nuclear reflections of space group $I4_1/acd$ are also observed in a wide temperature range from 4 K to 600 K, which suggests a reduced crystal structure symmetry. This neutron-scattering work provides a direct, well-refined experimental characterization of the magnetic and crystal structures that are crucial to the understanding of the unconventional magnetism exhibited in this unusual magnetic insulator.

DOI: 10.1103/PhysRevB.87.140406 PACS number(s): 75.25.−j, 61.05.F−, 71.70.Ej

The 5d-based iridates have continuously provided a fertile playground for the studies of novel physics driven by the spin-orbit interaction (SOI). It is believed that SOI (0.4–1 eV), which is proportional to Z^4 (Z is the atomic number), plays a critical role in the iridates and rigorously competes with other relevant energies, particularly the on-site Coulomb interaction U (0.4–2.5 eV), which is significantly reduced because of the extended nature of the 5d orbitals. A new balance between the competing energies is, therefore, established in the iridates and drives exotic quantum phases. Recent experimental observations and theoretical proposals for the iridates have captured the intriguing physics driven by SOI and examples include the following: the $J_{\text{eff}} = 1/2$ Mott state,[1–4] superconductivity,[5,6] a correlated topological insulator with large gaps,[7,8] spin liquid in a hyperkagome structure,[9] Weyl semimetal with Fermi arcs,[10] the Kitaev mode,[11,12] and three-dimensional (3D) spin liquid with Fermionic spinons.[13]

Among all the iridates studied, the single-layer Sr_2IrO_4 has been subjected to the most extensive investigations due to its structural and electronic similarities to the undoped high-T_C cuprates such as La_2CuO_4. This magnetic insulator was proposed to be an effective $J_{\text{eff}} = 1/2$ Mott-Hubbard state arising from the SOI.[1,3] Although the insulating ground state has been established by angle-resolved photoemission spectroscopy[1] and resonant x-ray scattering (RXS) measurements,[3] some critical insights into the crystal and magnetic structures remain conspicuously elusive. For example, the strong SOI limit $J_{\text{eff}} = 1/2$ ground-state scenario has been recently challenged by x-ray absorption spectroscopy,[14] time-resolved optical studies,[15] and theory.[16] The nature of the weak ferromagnetism arising from the canted antiferromagnetic (AFM) order is not fully characterized experimentally. This is primarily due to the lack of large single crystals and the strong absorbing cross section of the Ir ions that prevent a comprehensive neutron study. Here we report the results of a neutron diffraction investigation of single-crystal Sr_2IrO_4. The central findings of this work are the following: (1) The magnetic and crystal structures are completely determined; (2) the system undergoes an antiferromagnetic transition at 224(2) K with an ordered moment of 0.208(3) μ_B/Ir site and a canted spin configuration within the basal plane; and (3) the spin orientation is intimately associated with the rotation of the IrO_6 octahedra, which results in 0.202(3) and 0.049(2) μ_B/Ir site for the a axis and the b axis, respectively. In addition, nuclear reflections incompatible with the previously reported space group (SG) are observed and indicate a possible lowering of the structural symmetry.

The Sr_2IrO_4 single crystal studied ($2 \times 2 \times 1$ mm^3, mass = 8 mg) was grown using self-flux techniques.[17] Because the iridium is highly neutron absorbing, the equal-dimensional shaped crystal simplifies the necessary absorption correction.[18] The neutron diffraction measurements were carried out at the HB1A, HB1 triple axis spectrometers, and the HB3A four circle diffractometer at the High Flux Isotope Reactor at the Oak Ridge National Laboratory. For the measurements using triple axis spectrometers, the crystal was aligned in the $(h,0,l)$, (h,h,l), $(0,k,l)$ and other scattering planes to probe various magnetic reflections. A closed-cycle refrigerator and high temperature furnace were employed to monitor the T dependence of the magnetic and nuclear reflections.

Sr_2IrO_4 was reported to crystallize in a tetragonal structure (SG $I4_1/acd$, No. 142) with $a = b = 5.484$ Å and $c = 25.83$ Å at 4 K.[19,20] With reflection conditions compliant with the $I4_1/acd$ symmetry, we have collected 137 nuclear reflections of Sr_2IrO_4 using HB3A for structure refinements. The most prominent features of the crystal structure are the elongation of the IrO_6 octahedra along the c axis (2.055 Å for the out-of-plane distance compared to 1.981 Å in-plane), and the rotation of the octahedra with respect to the c axis about 11.8(1)° at 4 K. This leads to a $\sqrt{2} \times \sqrt{2}$ expansion of unit cell in the basal plane compared to the higher symmetry Sr_2RuO_4 [Fig. 1(a)].

The antitranslation in combination with the body centering dictates a (1,1,1) magnetic propagation wave-vector, as discussed previously.[16,21] Figure 2(a) displays the T dependence of the Bragg intensity ($I_B \propto |M_s|^2$, M_s is the order parameter) of the magnetic reflection (1,0,2). The intensity vanishes around $T_N = 224(2)$ K and is consistent with the

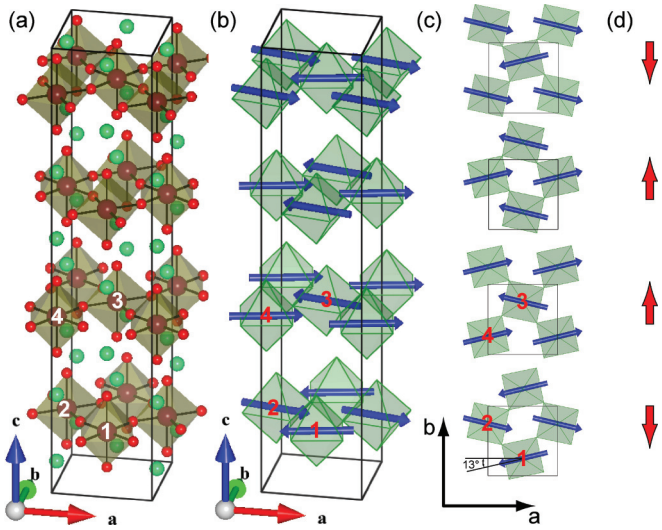

FIG. 1. (Color online) (a) The crystal structure of Sr_2IrO_4 with SG $I4_1/acd$ (setting 2). Each IrO_6 octahedron rotates 11.8° about the c axis. The Ir atoms of the nonprimitive basis are labeled 1, 2, 3, and 4 plus the body centering translation (1/2,1/2,1/2). (b) The refined magnetic structure from single-crystal neutron diffraction measurements. (c) The same spin configuration projected on the basal planes. (d) The net moment projected along the b axis for individual layers.

TABLE I. Basis vectors (BVs) for the SG $I4_1/acd$ with magnetic propagation vector $\mathbf{k} = (1,1,1)$. The decomposition of the magnetic representation is $\Gamma_{\rm mag} = 2\Gamma_1^2 + 2\Gamma_2^2 + 2\Gamma_3^1 + 2\Gamma_4^1$. The atoms of the nonprimitive basis are located at 1:(1/2,1/4,1/8), 2:(0,3/4,1/8), 3:(1/2,3/4,3/8), 4:(0,1/4,3/8) (Fig. 1). For clarity, only the in-plane BVs are listed.

			Component						Component		
IR	BV	Atom	m_a	m_b	m_c	IR	BV	Atom	m_a	m_b	m_c
Γ_1	ψ_1	1	1	0	0	Γ_2	ψ_5	1	1	0	0
		2	1	0	0			2	1	0	0
		3	1	0	0			3	−1	0	0
		4	1	0	0			4	−1	0	0
	ψ_2	1	0	1	0		ψ_6	1	0	1	0
		2	0	1	0			2	0	1	0
		3	0	−1	0			3	0	1	0
		4	0	−1	0			4	0	1	0
	ψ_3	1	1	0	0		ψ_7	1	1	0	0
		2	−1	0	0			2	−1	0	0
		3	1	0	0			3	−1	0	0
		4	−1	0	0			4	1	0	0
	ψ_4	1	0	1	0		ψ_8	1	0	1	0
		2	0	−1	0			2	0	−1	0
		3	0	−1	0			3	0	1	0
		4	0	1	0			4	0	−1	0

magnetization measurement.[17] Fitting the order parameter to the power-law scaling function $I_B \approx |t|^{2\beta}$, where $t = 1 - T/T_N$ is the reduced temperature, leads to the critical exponent $\beta = 0.18(1)$. It apparently deviates from the $\beta = 0.325$ expected for a $3D$ Heisenberg spin system. Figures 2(b) and 2(c) illustrate the wave-vector scans within and perpendicular to the basal plane at several temperatures. In both cases, the lineshape of the magnetic scattering evolves into a Gaussian profile below T_N, signaling the formation of the long-range magnetic order. Our observation is in accord with the RXS studies indicating that a short-range Heisenberg spin fluctuation occurs only in a paramagnetic state.[22]

A quantitative characterization of the magnetic structure and moment size of the Ir^{4+} ions can be obtained by a comprehensive survey of the magnetic reflections in conjunction with the model calculation. Figure 3 shows the neutron diffraction scans at selected reflections. The disappearance of the scattering above T_N and decrease in intensity at large momentum transfer indicate their magnetic nature. Differing from the early RXS studies where the magnetic reflections are present only at $(0,1,4n+2)$ and $(1,0,4n)$,[3] our neutron diffraction shows additional Bragg peaks at the $(0,1,4n)$ and $(1,0,4n+2)$ positions. The nearly identical intensity at equivalent wave-vectors (1,0,2) and (0,1,2) indicates the crystal has equally populated magnetic domains. Note that the structural refinement with the same sample cannot determine whether the system is structurally twinned.[23] The presence of both types of reflections strongly suggests that they originate from the twinned crystallographic domains. According to the Landau theory, the symmetry properties of the magnetic structure can be described by only one irreducible representation (IR). With Ir ions located at the 8a Wyckoff positions for the SG $I4_1/acd$ and the propagation wave-vector $q_M = (1,1,1)$, the magnetic representation can be decomposed into $\Gamma_{\rm mag} = 2\Gamma_1^2 + 2\Gamma_2^2 + 2\Gamma_3^1 + 2\Gamma_4^1$, where Γ_1, Γ_2 are the two-dimensional IRs with basis vectors lying in the ab plane and Γ_3, Γ_4 are the one-dimensional IRs with moments pointing parallel to the c axis. Since the magnetic susceptibility suggests that the spin easy axis lies in the basal plane,[17] we exclude spin configurations associated with Γ_3 and Γ_4 in the analysis. Table I lists the basis vectors of IRs Γ_1 and Γ_2. In particular, the spin structure based on linear combination of $\psi(2)$ and $\psi(3)$ of Γ_1 has a $(+-+-)$ configuration along the a axis (or the M4 structure described in Refs. 16 and 21) and $(++--)$ along the b axis for the labeled Ir ions in Fig. 1. In contrast, the linear combination of $\psi(5)$ and $\psi(8)$ in Γ_2 gives $(++--)$ along the a axis and $(+-+-)$ along the b axis (the M3 configuration). These spin structures derived from representation analysis using BasIreps program[24] are in accord with the results from previous neutron powder diffraction.[21]

Table II compares the expected intensities for the two relevant spin models and the experimental observations. The M4 and M3 configurations each have distinct distributions of magnetic scattering intensities.[26] For example, the collinear structure with a axis $(+-+-)$ components produces the strongest scattering at the (0,1,2) reflection and gives zero intensity at the (1,0,0) Bragg point. However, the $(++--)$ collinear state associated with the M3 configuration will generate the strongest scattering at the (1,0,0) peak, which is not observed experimentally. The neutron diffraction results shown in Table II clearly support the M4 spin configuration and confirm the previous neutron diffraction work on the powder sample.[21] To test whether there are additional canted moments along the b axis with the $(++--)$ configuration within Γ_1, we probed the scattering at the expected $(0,0,2n+1)$ reflections. Figures 3(d) and 3(e) display the scans at the (0,0,3)

TABLE II. Comparison of observed and calculated magnetic intensities from two symmetry compatible spin models. To get the scale factor, separate sets of nuclear reflections were collected at HB3A with incident neutron wavelength of 1.5424 and 1.003 Å, respectively. Additional 37 nuclear reflections were collected at HB1A for intensity normalization.[25]

Reflection	Observation	M4 model	M3 model
(0,0,3)	0.26 ± 0.03	0.25	0.25
(0,0,5)	0.20 ± 0.03	0.20	0.20
(1,1,1)	0.08 ± 0.07	0.08	0.08
(0,1,2)	6.80 ± 0.17	6.99	1.05
(0,1,6)	4.72 ± 0.32	4.50	2.73
(1,0,2)	6.99 ± 0.18	6.99	1.05
(1,0,4)	2.33 ± 0.22	2.48	5.81
(1,0,6)	4.72 ± 0.32	4.51	2.73
(1,0,8)	2.56 ± 0.32	2.28	3.01
(1,0,14)	0.88 ± 0.21	0.54	0.48
(1,0,16)	0.18 ± 0.09	0.24	0.26
(1,2,0)	1.53 ± 0.36	1.76	0.43
(1,2,4)	1.14 ± 0.23	1.46	0.52
(1,2,8)	0.85 ± 0.12	0.82	0.45

and (0,0,5) Bragg peaks. Although much weaker, the magnetic scattering is clearly present at low T and confirms the staggered AFM order propagating along the c axis. A total of 14 magnetic reflections combined with 137 nuclear reflections allow an accurate determination of the spin structure and the associated moment. Using the M4 spin model and the magnetic form factor for Ir^{4+},[27] we have obtained $m_a = 0.202(3)\mu_B$ along the a axis and $m_b = 0.048(2)\mu_B$ along the b axis, yielding a total moment of $0.208(3)\mu_B/Ir^{4+}$ site. This value is smaller than $0.36(6)\ \mu_B$ from a recent single crystal neutron-scattering study[28] but quite consistent with the powder neutron diffraction results in which the upper limit of the moment does not exceed $0.29(4)\ \mu_B$.[21] The magnetic configuration in Figs. 1(b)–1(d) show that spins projected along the b axis have a staggered $\downarrow\uparrow\uparrow\downarrow$ pattern along the c axis, with Ir spins deviating 13(1)° away from the a axis [see Fig. 1(d)]. This spin canting rigidly tracks the staggered octahedral rotation, as illustrated in a previous RXS study.[1] This remarkable correlation proves the existence of strong magnetoelastic coupling in the iridate, which is also suggested in experimental studies of transport and magnetic properties of the system.[4,29]

Theoretically, the spin Hamiltonian in the strong SOI limit includes the isotropic coupling (J) and the Dzyaloshinsky-Moriya interaction (D) caused by the lattice distortion.[11]

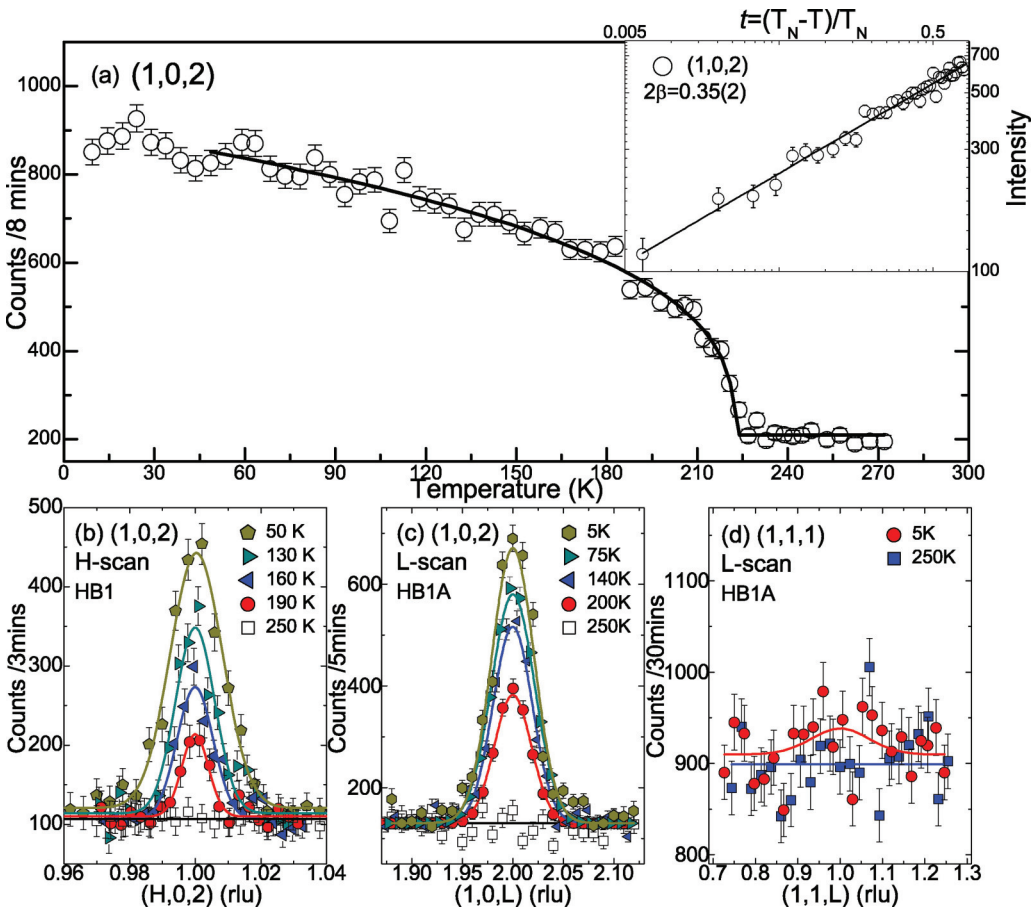

FIG. 2. (Color online) (a) The T-dependence of the magnetic (1,0,2) reflection. Inset shows the intensity versus the reduced temperature ($t = |1 - T/T_N|$) in logarithmic scale. The wave-vector scan along (b) the [H,0,0] and (c) the [0,0,L] directions for the (1,0,2) peak at selected temperatures that probe the in-plane and out-of-plane correlations. (d) Similar wave-vector scans for the magnetic (1,1,1) reflection above and below T_N. Note that the counting time is 10 times compared to those of the strong (1,0,2) peak.

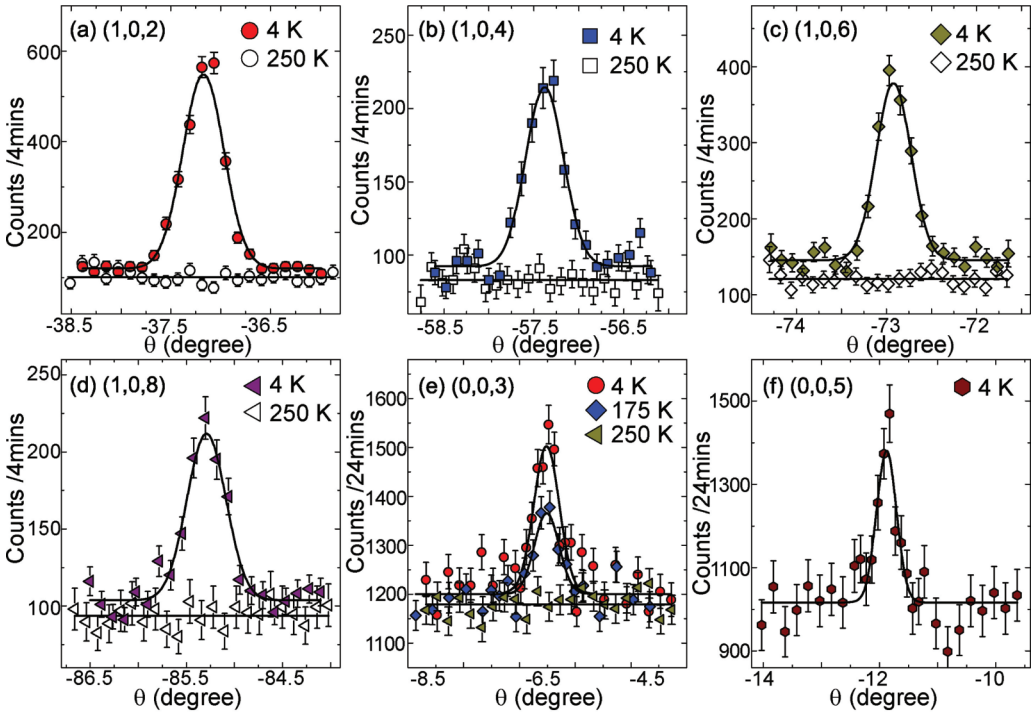

FIG. 3. (Color online) Selected rocking scans at 4 K and 250 K for the (a) (1,0,2), (b) (1,0,4), (c) (1,0,6), (d) (1,0,8), (e) (0,0,3), and (f) (0,0,5) magnetic reflections. The weaker $(0,0,2n+1)$ are measured with much longer counting time.

The spin canting is governed by the ratio of D and J and is solely determined by the lattice distortion. This explains the relatively large spin canting in the $5d$ system compared to that in La_2CuO_4 where SOI is insignificant (SOI $\propto Z^4$, $Z = 29$ and 77 for Cu and Ir, respectively). The measured magnetic moment is much smaller than 1 μ_B conventionally anticipated for a $S = 1/2$ system but is similar to those of other iridates, such as Na_2IrO_3 and $BaIrO_3$, where the saturated moment is less than 20% of 1 μ_B/Ir.[17,30] The significantly reduced moment might be attributed to the strong hybridization of the Ir $5d$ orbital with the ligand oxygen $2p$ orbital because of the large spatial extend of $5d$ wave functions or the axial distortion of IrO_6 octahedra away from the cubic symmetry.[16,21] Although the latter has been invoked to explain the reduced moment, it is inconsistent with the branching ratio (BR) obtained from the x-ray absorption spectrum.[31,32] The reduced $\langle \mathbf{S} \cdot \mathbf{L} \rangle$ caused by the decreased moment makes the corresponding BR values far too small compared to the measured one. It was argued that the moment value and BR are irreconcilable using only one t_{2g} electron and $j = 5/2$. For instance, Laguna-Marco *et al.* have shown in a multielectron simulation in $BaIrO_3$ that $J_{\text{eff}} = 1/2$ accounts for only half of $\langle \mathbf{S} \cdot \mathbf{L} \rangle$ required in BR to match the experimental determined value, while the remaining half is induced by spin-orbit mixing of the t_{2g} and e_g states.[33]

The observation of the magnetic $(0,1,4n+2)$ and $(1,0,4n)$ indicates either the breakdown of the tetragonal symmetry of the system or a weak coupling between the magnetic and lattice degrees of freedom. To understand the possible structural origin of the anomalous magnetic behavior, we have surveyed extensively in reciprocal space and observed the presence of nuclear reflections $(oddh,0,oddl)$ that are not allowed in SG $I4_1/acd$. Similar behavior is also observed in a recent single crystal neutron diffraction work.[28] Figure 4(b) shows the rocking scans of the (0,1,1) reflection at selected temperatures. The intensity continuously decreases on warming and shows no sign of transition to 600 K. The reduction in intensity cannot be accounted by the thermal vibration of the elements (Debye-Waller factor). The lack of anomaly near T_N is also consistent with the transport,[17,34] thermodynamic,[29] and optical conductivity studies.[2,15] Scans across other Bragg peaks of (1,0,1) and (1,0,5) display similar violation of the required $(h = 2n,0,l = 2n)$ reflection condition. Although it cannot be completely ruled out that the forbidden peaks might be due to the structural defects such as oxygen vacancies commonly observed in oxides, the systematically enhanced intensities of these forbidden peaks with isovalent Rh doping[35] suggest it is an intrinsic property. If the observed forbidden peaks arise from the reduced crystal symmetry, they would lead to possible nonisomorphic subgroups of either $I4_1/a22$ (No. 98) or $I4_1/a$ (No. 88) due to the absent c- and d-glide planes. The absence of scattering across the (1,1,0) reflection further rules out the SG of $I4_1/a22$. Such observation of reduced structural symmetry that persists at a much higher temperature than T_N, implies the formation of a crystallographic template for the low-T spin structure that changes the tetragonal symmetry. This observation is certainly intriguing and the origin of it remains to be understood.

It is established that the magnetic and electronic properties are highly susceptible to slight impurity doping for Sr, Ir, or oxygen.[4,29,36–38] For example, doping Mn results in a spin-flop transition with moments aligning along the c axis.[36] The remaining $J_{\text{eff}} = 1/2$ state revealed by RXS measurement suggests its robustness against the alternation of spin structure.

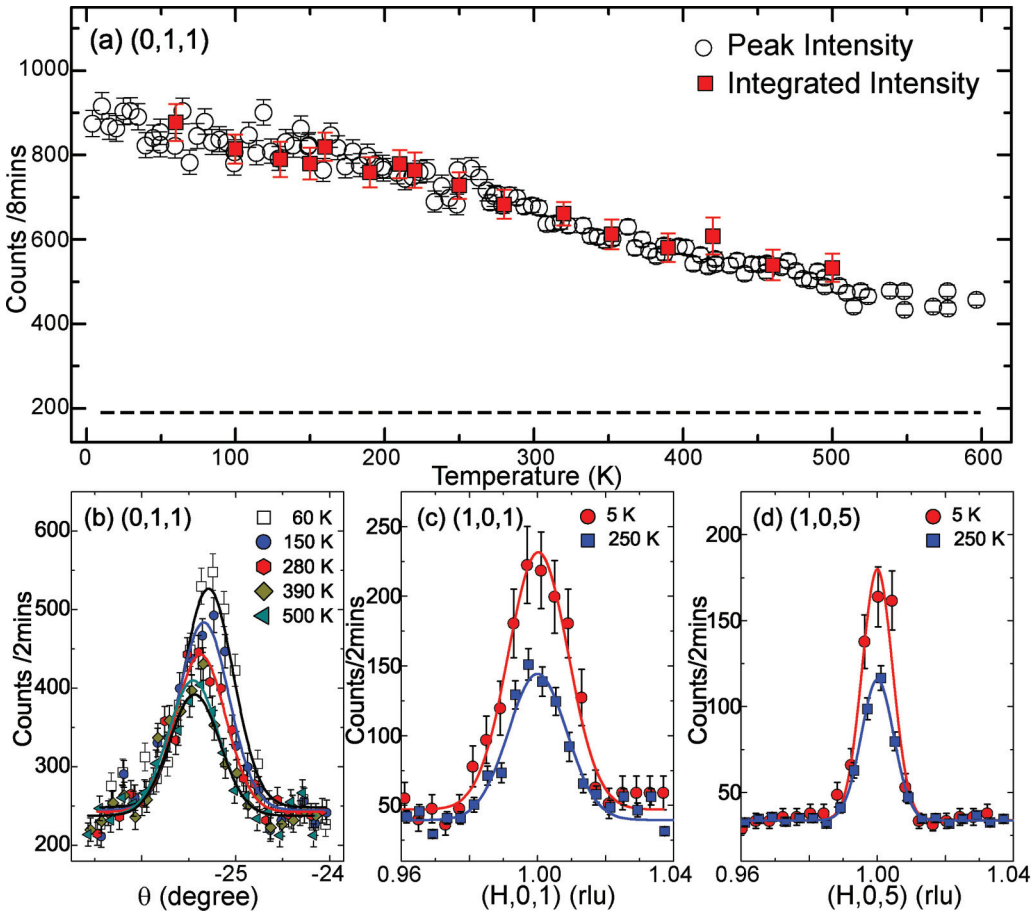

FIG. 4. (Color online) (a) The T-dependence of the structural (0,1,1) reflection. Open circles are the peak intensity and solid squares the integrated intensity. Dashed line is the background derived from the Gaussian fit to the rocking scan. (b) The rocking scans of the (0,1,1) peak at $T = 60$, 150, 280, 390, and 500 K. The wave-vector scans along the [1,0,0] direction for (c) the (1,0,1) and (d) the (1,0,5) reflections at 5 K and 250 K.

On the other hand, replacing Ir with isovalent Rh^{4+} leads to a rich phase diagram of metal-insulator transition tuned by SOI.[37] The transition was explained by the effective reduction of the splitting between the $J_{\text{eff}} = 1/2$ and $J_{\text{eff}} = 3/2$ bands due to the reduced SOI; this in turn alters the relative strength of the SOI and the crystal electric field (CEF) that dictates the magnetic state. This notion is also consistent with a recent theoretical proposal that the change of CEF associated with the underlying structure could be critical to determine the magnetic ground states. The present single-crystal neutron diffraction unambiguously determines the magnetic structure and proves the rigid coupling of the spin canting with the rotation of the IrO_6 octahedra. These findings finally fill the longstanding gap in our understanding of the magnetic properties in Sr_2IrO_4, an archetype of the $J_{\text{eff}} = 1/2$ insulators.

We thank Q. Huang, S. Lovesey, D. Khalyavin, and G. Khaliullin for invaluable discussions. Research at ORNL's High Flux Isotope Reactor was sponsored by the Scientific User Facilities Division, Office of Basic Energy Sciences, US Department of Energy. The work at University of Kentucky was supported by NSF through Grants No. DMR-0856234 and No. EPS-0814194.

[1]B. J. Kim *et al.*, Phys. Rev. Lett. **101**, 076402 (2008).
[2]S. J. Moon, H. Jin, W. S. Choi, J. S. Lee, S. S. A. Seo, J. Yu, G. Cao, T. W. Noh, and Y. S. Lee, Phys. Rev. B **80**, 195110 (2009).
[3]B. J. Kim *et al.*, Science **323**, 1329 (2009).
[4]M. Ge, T. F. Qi, O. B. Korneta, D. E. DeLong, P. Schlottmann, W. P. Crummett, and G. Cao, Phys. Rev. B **84**, 100402 (2011).
[5]F. Wang and T. Senthil, Phys. Rev. Lett. **106**, 136402 (2011).
[6]Y. Z. You, I. Kimchi, and A. Vishwanath, Phys. Rev. B **86**, 085145 (2012).
[7]A. Shitade, H. Katsura, J. Kunes, X. L. Qi, S. C. Zhang, and N. Nagaosa, Phys. Rev. Lett. **102**, 256403 (2009).
[8]C. H. Kim, H. S. Kim, H. Jeong, H. Jin, and J. Yu, Phys. Rev. Lett. **108**, 106401 (2012).

[9]Y. Okamoto, M. Nohara, H. Aruga-Katori, and H. Takagi, Phys. Rev. Lett. **99**, 137207 (2007).

[10]X. G. Wan, A. M. Turner, A. Vishwanath, and S. Y. Savrasov, Phys. Rev. B **83**, 205101 (2011).

[11]G. Jackeli and G. Khaliullin, Phys. Rev. Lett. **102**, 017205 (2009).

[12]Y. Singh, S. Manni, J. Reuther, T. Berlijn, R. Thomale, W. Ku, S. Trebst, and P. Gegenwart, Phys. Rev. Lett. **108**, 127203 (2012).

[13]Y. Zhou, P. A. Lee, T. K. Ng, and F. C. Zhang, Phys. Rev. Lett. **101**, 197201 (2008).

[14]D. Haskel, G. Fabbris, M. Zhernenkov, P. P. Kong, C. Q. Jin, G. Cao, and M. van Veenendaal, Phys. Rev. Lett. **109**, 027204 (2012).

[15]D. Hsieh, F. Mahmood, D. H. Torchinsky, G. Cao, and N. Gedik, Phys. Rev. B **86**, 035128 (2012).

[16]L. C. Chapon and S. W. Lovesey, J. Phys.-Condes. Matter **23**, 252201 (2011).

[17]G. Cao, J. Bolivar, S. McCall, J. E. Crow, and R. P. Guertin, Phys. Rev. B **57**, R11039 (1998).

[18]The absorption corection factor has been numerically applied to the collected reflections based on the sample shape. The mean transmission (T) is 0.92 with the minimum at the (0, 0, 8) reflection ($T = 0.79$) and the maximum at the (2, 1, 1) peak ($T = 0.95$).

[19]Q. Huang *et al.*, J. Solid State Chem. **112**, 355 (1994).

[20]M. K. Crawford, M. A. Subramanian, R. L. Harlow, J. A. Fernandez-Baca, Z. R. Wang, and D. C. Johnston, Phys. Rev. B **49**, 9198 (1994).

[21]S. W. Lovesey *et al.*, J. Phys.: Condens. Matter **24**, 496003 (2012).

[22]S. Fujiyama, H. Ohsumi, T. Komesu, J. Matsuno, B. J. Kim, M. Takata, T. Arima, and H. Takagi, Phys. Rev. Lett. **108**, 247212 (2012).

[23]Our neutron diffraction measurement typically has beam size of 5×5 mm at the sample position and is larger than the $10 \sim 100\,\mu$m used in the RXS experiment that is comparable with magnetic domain size. See, for example, S. Boseggia, R. Springell, H. C. Walker, A. T. Boothroyd, D. Prabhakaran, D. Wermeille, L. Bouchenoire, S. P. Collins, and D. F. McMorrow, Phys. Rev. B **85**, 184432 (2012).

[24]J. Rodriguez-Carvajal, Physica B **192**, 55 (1993).

[25]The nulcear reflections are collected using two-axis mode, while the magnetic reflections are collected using three-axis mode to improve the signal-to-noise ratio. The corresponding integrated intensities are corrected using the method described by R. Pynn, Acta Cryst. B **31**, 2555 (1975).

[26]Because of the tetragonal symmetry of the crystal structure, the linear combination of $\psi(1)$ and $\psi(4)$ within the same Γ_1 IR can also describe the observed intensities. For simplicity, we use $\psi(2)$ and $\psi(3)$ to be consistent with the spin configuration reported in Ref. 21.

[27]K. Kobayashi, T. Nagao, and M. Ito, Acta Crystallogr. Sect. A **68**, 589 (2012).

[28]C. Dhital *et al.*, Phys. Rev. B **87**, 144405 (2013).

[29]S. Chikara, O. Korneta, W. P. Crummett, L. E. DeLong, P. Schlottmann, and G. Cao, Phys. Rev. B **80**, 140407 (2009).

[30]F. Ye, S. Chi, H. Cao, B. C. Chakoumakos, J. A. Fernandez-Baca, R. Custelcean, T. F. Qi, O. B. Korneta, and G. Cao, Phys. Rev. B **85**, 180403 (2012).

[31]J. P. Clancy, N. Chen, C. Y. Kim, W. F. Chen, K. W. Plumb, B. C. Jeon, T. W. Noh, and Y. J. Kim, Phys. Rev. B **86**, 195131 (2012).

[32]G. van der Laan and B. T. Thole, Phys. Rev. Lett. **60**, 1977 (1988).

[33]M. A. Laguna-Marco, D. Haskel, N. Souza-Neto, J. C. Lang, V. V. Krishnamurthy, S. Chikara, G. Cao, and M. van Veenendaal, Phys. Rev. Lett. **105**, 216407 (2010).

[34]N. S. Kini, A. M. Strydom, H. S. Jeevan, C. Geibel, and S. Ramakrishnan, J. Phys.-Condens. Matter **18**, 8205 (2006).

[35]F. Ye, S. Chi, B. C. Chakoumakos, J. A. Fernandez-Baca, T. F. Qi, and G. Cao (2013) (unpublished).

[36]S. Calder, G. X. Cao, M. D. Lumsden, J. W. Kim, Z. Gai, B. C. Sales, D. Mandrus, and A. D. Christianson, Phys. Rev. B **86**, 220403(R) (2012).

[37]T. F. Qi, O. B. Korneta, L. Li, K. Butrouna, V. S. Cao, X. Wan, P. Schlottmann, R. K. Kaul, and G. Cao, Phys. Rev. B **86**, 125105 (2012).

[38]O. B. Korneta, T. Qi, S. Chikara, S. Parkin, L. E. DeLong, P. Schlottmann, and G. Cao, Phys. Rev. B **82**, 115117 (2010).